Coastal Engineering 71 (2013) 102–118

Contents lists available at SciVerse ScienceDirect

Coastal Engineering

journal homepage: www.elsevier.com/locate/coastaleng

Realistic wave generation and active wave absorption for Navier–Stokes models Application to OpenFOAM®

Pablo Higuera, Javier L. Lara, Inigo J. Losada *

Environmental Hydraulics Institute "IH Cantabria", Universidad de Cantabria, C/Isabel Torres no. 15, Parque Cientifico y Tecnologico de Cantabria, 39011 Santander, Spain

ARTICLE INFO

Article history:
Received 26 February 2012
Received in revised form 2 June 2012
Accepted 29 July 2012
Available online 1 September 2012

Keywords:
CFD
OpenFOAM
Wave generation
Wave absorption
Two phase flow

ABSTRACT

The present paper and its companion (Higuera et al., 2012) introduce OpenFOAM® as a tool to consider for coastal engineering applications as it solves 3D domains and considers two-phase flow. In this first paper, OpenFOAM® utilities are presented and the free surface flow solvers are analysed. The lack of specific boundary conditions for realistic wave generation is overcome with their implementation combined with active wave absorption. Wave generation includes all the widely used theories plus specific piston-type wavemaker replication. Also standalone active wave absorption implementation is explained for several formulations, all of which are applicable to 3D cases. Active wave absorption is found to enhance stability by decreasing the energy of the system and to correct the increasing water level on long simulations. Furthermore, it is advantageous with respect to dissipation zones such as sponge layers, as it does not increase the computational domain. The results vary depending on the theory (2D, Quasi-3D and 3D) but overall performance of the implemented methods is very good. The simulations and results of the present paper are purely theoretical. Comparisons with laboratory data are presented in the second paper (Higuera et al., 2012).

1. Introduction

Eulerian three-dimensional NS solvers imply a new insight in physics as they allow a correct representation of the wave processes, including the simulation of real sea states in which random waves show directionality. But the new dimension has to be discretised as well, which makes the size of the computational domain to increase dramatically. Such growth most of the times results in a need to parallelise the models in order to accelerate the solving process and make it suitable for practical applications. Several examples can be found in Lubin et al. (2003), Li et al. (2004), Christensen (2006), Hur et al. (2008), Wang et al. (2009) or Lara et al. (2012) and del Jesus et al. (2012). With decreasing simulation times and cost per simulation, three-dimensional models applied to larger domains are affordable now.

Why OpenFOAM®? Because it is a robust and advanced CFD code widely used in the industry. Furthermore, it is open source, so it is available for free and can be modified. It is also well documented and it has a large and active community of users. Regarding coastal engineering purposes, it supports two phase flows with several turbulence models out of the box. However, it is not adapted to deal with most coastal engineering simulations as it lacks specific boundary conditions for realistic wave generation and active absorption (Lara et al., 2011) or porous media as other 3D models recently available: Lara et al. (2012) and del Jesus et al. (2012). Other models available have been used for similar purposes, for example ComFLOW®, which offers two phase flow simulations of waves with active wave absorption (Luppes et al., 2010). Nevertheless, its computational scheme is less robust, because it relies in the cutting cell method, which can have less computational cost, but also involves a less realistic behaviour compared with the adaptative meshing method of OpenFOAM®.

Active wave absorption is widely known in the physical modelling field, as it is needed to cancel out reflected waves that reach the wavemaker (Christensen and Frigaard, 1994). There are several studies with different absorption theories, e.g., Christensen and Frigaard (1994), Schäffer and Klopman (2000) or Newman (2010). It has also been applied to numerical models as in Wellens et al. (2009), Luppes et al. (2010), Lara et al. (2011) or Wellens (2012). Wave generation in numerical models requires the use of special boundary conditions linked with active absorption to study the processes correctly, as it prevents from effects such as the increment of energy in the domain and the rising of the mean water level. For example, the water level increases due to the excess in mass in the wave crests, which is unbalanced with the water extraction in the troughs (see Fig. 3 in Torres-Freyermuth et al. (2010) as an example). Porous media or numerical damping zones may also be used, but they are known to produce an increment in the mean water level due to the existence of a dissipative medium (Mendez et al., 2001). This variation modifies the wave dynamics, generating wave reflection. On top of that, they require adding large zones (Wei and Kirby, 1995) to the domain, on the order of several wave lengths, which may be even larger than the initial domain itself, increasing the computational cost. Active

* Corresponding author. Tel.: +34 942 20 16 16; fax: +34 942 20 18 10.
E-mail address: losadai@unican.es (I.J. Losada).

0378-3839/$ – see front matter © 2012 Elsevier B.V. All rights reserved.
http://dx.doi.org/10.1016/j.coastaleng.2012.07.002

wave absorption allows wave energy to flow out and maintains the water level without the inconvenience of enlarging the domain, and ensuring desired energy levels during the simulations.

The purpose of this paper is the implementation of wave generation and absorption theories in OpenFOAM® with the aim of presenting a robust 3D, two-phase numerical tool for practical applications in coastal engineering.

The present paper is structured as follows. After this brief introduction, a description of OpenFOAM® model is given. Following that, the theory behind the new boundary conditions for wave generation and absorption and the implementation process are detailed. The model is validated next against theoretical applications in order to prove the performance and stability of the newly implemented simultaneous wave generation and active absorption system. A detailed validation of the new OpenFOAM® boundary conditions against laboratory experimental data, covering an ample range of different coastal engineering processes is presented in a companion paper Higuera et al. (in press). To conclude, some conclusions are remarked.

2. Description of OpenFOAM®

In the following section, a brief overview of the OpenFOAM® toolbox is given first. Then more specific information about the two-phase solvers, which are the most relevant for coastal engineering, is presented. This includes a brief description and the numerical implementation.

2.1. General overview

OpenFOAM®[1] (*Open* Field *O*peration *A*nd *M*anipulation) is a free and open source CFD toolbox. Basically it is a bundle of C++ libraries and codes to solve complex problems such as turbulence, fluid flows, electromagnetics, chemical reactions, combustion… using finite volume discretisation. It also features several applications to pre- and post-process the cases, including mesh generation tools ("blockMesh", "snappyHexMesh"), setting field values, mesh decomposition, sampling data (isosurfaces, gauges). OpenFOAM® is prepared to run cases in parallel, allowing an easy set up and a straightforward calculation method, handling itself the decomposition process and the final (optional) reconstruction process.

As already mentioned it is written in C++, and furthermore it is object oriented, so its modular structure is an advantage to programme new solvers, boundary conditions or applications, allowing not to digging deeply in the source code to add new functionalities. This is a result of the data types and classes, specific of OpenFOAM®, which help to handle the fields in a more compact and easy way, avoiding unnecessary loops to do some operations.

Unlike commercial codes OpenFOAM® is not a black box, the user can control and modify each of the steps of the solving process by changing the source code. This is a great advantage, since several modules include data conversion from and to commercial CFD codes (Ansys®, Fluent®, CFX®) or formats (VTK), allowing cross validations. Other extended capabilities are added by third party programmes. The most representative case is undoubtedly Kitware's ParaView®, which is the main programme used for postprocessing purposes since it has two specific readers for native OpenFOAM® data.

2.2. "interFoam" solver

2.2.1. Description

"interFoam" is one of the solvers included in OpenFOAM®. It solves the three-dimensional Reynolds Averaged Navier–Stokes (RANS) equations for two incompressible phases using a finite volume discretisation and the volume of fluid (VOF) method. In VOF (Berberovic et al., 2009), each phase is described by a fraction α_i occupied by the volume of fluid of the ith material in the cell. Its principal advantages are that it is very simple, allowing very complex free surface configurations to be represented easily and that it involves no mesh motion. A minor disadvantage is that it becomes less effective as surface tension effects increase. However, most of the times in coastal engineering practical applications we are dealing with relatively long wave lengths, so that only for very specific phenomena surface tension forces are not negligible. It supports several turbulence models (e.g. $\kappa-\epsilon$, $\kappa-\omega$ SST, and LES).

"interFoam" solver is prepared for static meshes only. An enhanced version of it is "interDyMFoam", which handles dynamic meshes ("DyM" stands for it). Hence it can simulate floating body movements or dynamic mesh refinement along the free surface. Other than that it solves the same equations following the same procedures.

In this work several boundary condition modules have been implemented to work indistinctly with "interFoam" or "interDyMFoam". These add the capabilities of generating water waves according to multiple wave theories. On top of that, active wave absorption has been programmed based on extrapolated 2D theory to allow outgoing waves to flow away with minor reflection, either in pure absorbent boundaries or in wave generation ones. Furthermore, other theories have been developed in 3D to account for non orthogonal incident waves. Full details are given in the next section.

2.2.2. Governing equations

The aforementioned RANS equations, which include continuity (Eq. (1)) and mass conservation (Eq. (2)) equations, are the governing mathematical expressions which link pressure and velocity. The assumption of incompressible fluids has been used, which is applicable for most coastal engineering practical problems.

$$\nabla\cdot\mathbf{U}=0 \tag{1}$$

$$\frac{\partial\rho\mathbf{U}}{\partial t}+\nabla\cdot(\rho\mathbf{U}\mathbf{U})-\nabla\cdot\left(\mu_{eff}\nabla\mathbf{U}\right)=-\nabla p^{*}-\mathbf{g}\cdot X\nabla\rho+\nabla\mathbf{U}\cdot\nabla\mu_{eff}+\sigma\kappa\nabla\alpha \tag{2}$$

where all the bold letters indicate a vector field. ρ is the density, which is calculated as presented in Eq. (3); $\mathbf{U}$ is the velocity vector; p^{*} is the pseudo-dynamic pressure; $\mathbf{g}$ is the acceleration of gravity; $\mathbf{X}$ is the position vector. The last term on the right is the effect of surface tension: σ is the surface tension coefficient; κ is the curvature of the interface and is calculated as follows: $\kappa=\nabla\cdot\frac{\nabla\alpha}{|\nabla\alpha|}$, and α is the indicator function, which will be further commented later in this section. Finally μ_{eff} is the efficient dynamic viscosity, which takes into account the molecular dynamic viscosity plus the turbulent effects: $\mu_{eff}=\mu+\rho\nu_{turb}$. The newly introduced ν_{turb} is the turbulent kinetic viscosity, and it is given by the chosen turbulence model. The elements in Eq. (2) have a particular disposition: those placed on the left hand side of the equals sign are used in OpenFOAM® to assemble the coefficient matrix, and the ones on the right side are calculated explicitly and form the independent term of the equations.

An additional equation must also be taken into account to describe the movement of the phases. Since in the vast majority of coastal engineering applications only water and air are present, the following analysis is carried out for those two phases only. For a more general approach the reader is referred to Kissling et al. (2010). As a result of the assumption, just one indicator phase function (α) is needed, and defined as the quantity of water per unit of volume at each cell. This means that if $\alpha=1$ the cell is full of water, if $\alpha=0$ the cell is full of air, and in any other case it belongs to the interface. It is straightforward to calculate any of the properties of the fluid at

[1] http://www.openfoam.com/.

each cell, just by weighting them by the VOF function. For example, density of the cell is computed as follows:

$$\rho = \alpha\rho_{\text{water}} + (1-\alpha)\rho_{\text{air}}. \tag{3}$$

The starting point for the equation which tracks the fluid movement is a classic advection equation:

$$\frac{\partial\alpha}{\partial t} + \nabla\cdot\mathbf{U}\alpha = 0. \tag{4}$$

However, some restrictions apply in order to obtain physical results: a sharp interface must be maintained and α must be conserved and bounded between 0 and 1. OpenFOAM® makes use of an artificial compression term ($\nabla\cdot U_c\alpha(1-\alpha)$, (Weller, 2002)) instead of using a compressing differencing scheme. This approach is conservative and takes non-zero values only at the interface. Furthermore the flow is not compressed if $\mathbf{U_c}$ is normal to the interface $\left(\frac{\nabla\alpha}{|\nabla\alpha|}\right)$, which points towards greater values of α, and therefore from the air to the water phase. This yields the final expression:

$$\frac{\partial\alpha}{\partial t} + \nabla\cdot\mathbf{U}\alpha + \nabla\cdot\mathbf{U}_c\alpha(1-\alpha) = 0. \tag{5}$$

in which $|\mathbf{U}_c| = \min[c_\alpha|\mathbf{U}|, \max(|\mathbf{U}|)]$, where the user can specify factor c_α. By default it takes value 1, but it can be greater to enhance the compression of the interface. The boundedness of such equation is achieved by means of a especially designed solver called MULES (multidimensional universal limiter for explicit solution). It makes use of a limiter factor on the fluxes of the discretised divergence term to ensure a final value between 0 and 1. For further reference regarding the governing equations see Rusche (2002).

2.2.3. Solving procedure

Originally the solving algorithm was PISO (pressure implicit with splitting of operators), for a detailed description of the numerical solution of the equations see Kissling et al. (2010). More recent versions of the code have improvements. The new algorithm is called PIMPLE, as it is actually a mixture between PISO and SIMPLE (semi-implicit method for pressure-linked equations) algorithms. Its main structure is inherited from the original PISO, but it allows equation underrelaxation to ensure the convergence of all the equations at each time step. Both algorithms are thoroughly explained and applied for VOF in Jasak (1996).

A detailed flow chart, Fig. 1, has been developed in order to show the full loop for solving each time step. The main loop is presented with darker background. The alpha subcycle and the PIMPLE loop are further developed outside it. Both of them include the basic description of the newly developed boundary conditions. Within it, some variables (e.g. "nAlphaSubCycles", "nCorrectors"…) are defined. Those are specified in the programme control files and govern the performance of the model.

3. Implementation of the new boundary conditions

In the present section the structure of the boundary elements in which conditions are prescribed is presented first. For the wave generation and absorption boundary conditions (BCs), the theory behind them and the details of the numerical implementation are explained next.

All the newly generated BCs have been coded in the most general way, with the only assumption being that gravity always acts in the negative direction of the Z axis. They work in parallel and can handle structured or unstructured meshes, and even remeshing at each time step. Wave generation BC has been coded in a modular way, allowing the future addition of other wave theories in a very simple and almost automatic way.

As OpenFOAM® is a finite volume code, the BCs are specified at the faces. Each face at a boundary is owned by a unique cell. It is straightforward to access the face centre, the owner cell centre and all the faces and points which belong to it. The values for all the fields in those boundary faces or cells are also available. By using only this small amount of information, a great feedback can be obtained, which lays the foundations for stable and accurate wave generation and absorption.

3.1. Wave generation: theory

Wave generation is a critical point regarding numerical coastal engineering simulations. Generating waves is always the beginning of the vast majority of the cases we are dealing with. An accurate wave generation process lays the foundations of accurate final results. If the starting point is not accurate, all the errors introduced in this initial step will propagate until the end. Should this occur, the results may be completely different as wave interaction can show very important second order effects. Also the processes which affect waves, mainly shoaling and breaking, are highly influenced by wave shape and height. If those are not matched, chances are that the simulation will end up nowhere close to the physical solution.

Following this line, the built-in approach to fill the cells ("setFields") is very simplistic, as it only sets the VOF function with values 0 or 1 (dry or wet cells, this nomenclature will be further explained in Section 3.3). If the centre of the cell lies within the given domain it is filled with water, otherwise it is left as air. This has several implications, including that the initial water level may not be equal to the desired value and that where cells get refined close to the walls, water may reach a higher level, causing initial spurious waves. To solve this situation a new filling application has been developed to set VOF with values between 0 and 1 (dry, wet and partial cells) depending on the volume of the cell which lies within the specified domain. This approach allows a closer to reality start up, minimising the initial spurious waves.

Several boundary conditions for wave generation are currently available in literature. The first and oldest approach is GroovyBC, which is freely available online[2] and distributed independently from OpenFOAM®. While it is not a specific boundary condition for wave generation it accepts mathematical expressions in an elementary way. As a consequence, it is only suitable for simple wave theories as Stokes I or II, provided wave length is given or approximated explicitly. This approach is also rather simplistic, as it only accounts for wet/dry cells. The resulting waves show initial disturbances similar to steps due to this lack of partial cells, and need more time to regularise.

The second approach is the latest effort done, and it was recently presented in Jacobsen et al. (in press). Their approach is complete, accounting for wet, dry and also partial cells. However, they lack active wave absorption at the boundary, as they use relaxation zones. The technique has clear disadvantages as the existence of a wave damping region is known to produce an increment of the mean water level (Mendez et al., 2001). It also increases the computational domain by around two wave lengths (Wei and Kirby, 1995), which is quite inconvenient for already large domains and prototype applications.

The new wave generation BC presented in this paper introduces several new features as active wave absorption and a specific module to replicate laboratory wavemaker velocity profiles. It has been coded from scratch to realistically generate waves at the boundaries according to a number of wave theories, including: Stokes I, II and V, cnoidal and streamfunction regular waves; Boussinesq solitary wave; irregular (random) waves, first and second order; and piston-type wavemaker replication. To choose among wave generation theories it is advised to use the classic graph by Le Méhauté (1976).

[2] http://openfoamwiki.net/index.php/Contrib_groovyBC.

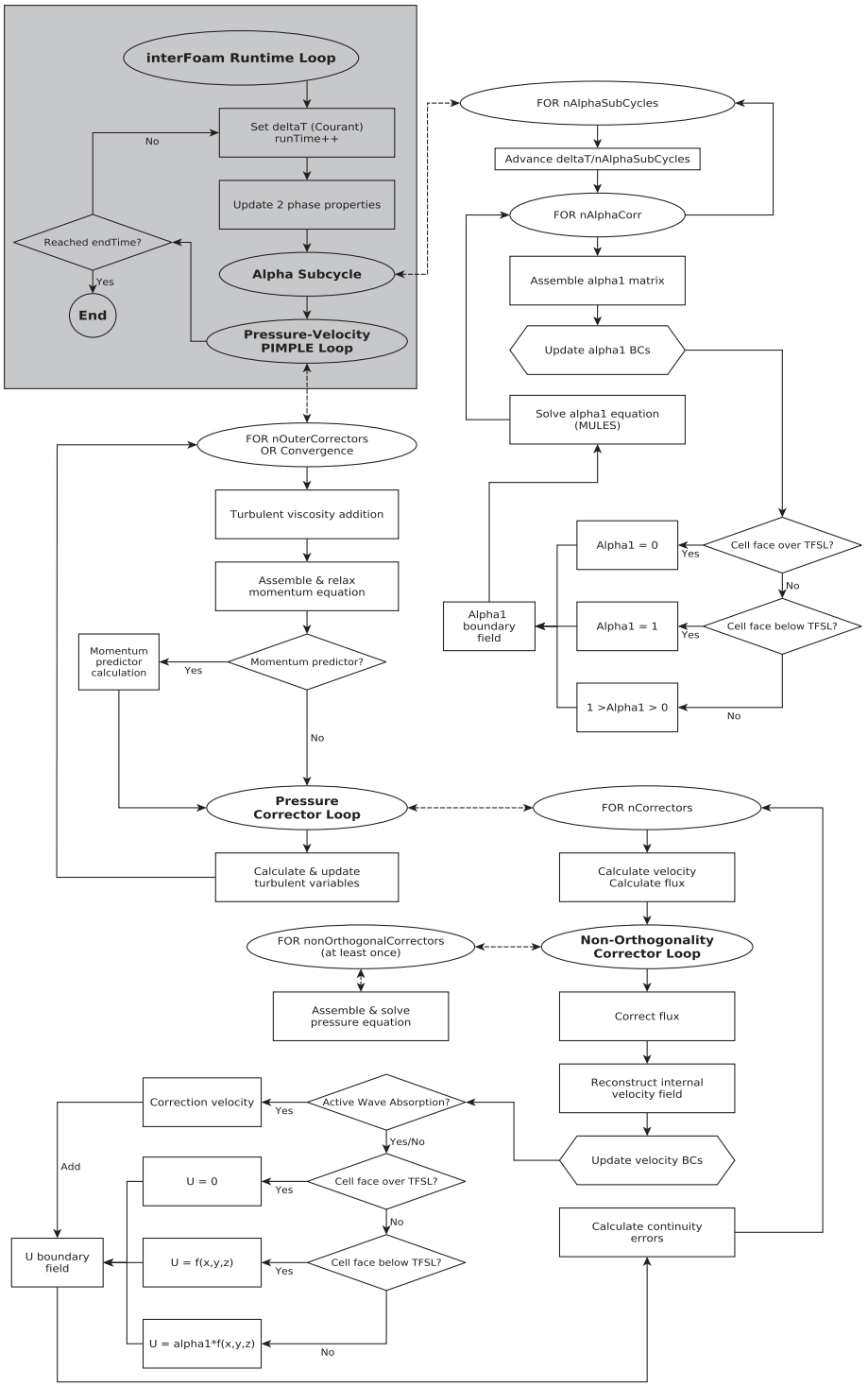

Fig. 1. "interFoam" solving flow chart. "TFSL" stands for theoretical free surface level.

As a convention for the wave generation BCs to work appropriately, gravity has to act in the negative direction of Z axis, and the lowest points of each wave generation boundary ("patch" in OpenFOAM®'s nomenclature) must be placed at the same level, but that level can be different from patch to patch. Angles are measured from the X axis, and increasing anticlockwise.

Each of the wave theories provides several analytical expressions to calculate free surface level and velocities for any coordinate (x, y, and z) in space. Only free surface (VOF function) and velocities are prescribed as Dirichlet BCs on the boundary, as if pressure was also set this way, the case will be overspecified. As shown later, pressure is calculated using a special boundary condition available in OpenFOAM®, which resembles a Neumann BC. As an example, the Stokes I theory expressions extended to 3D are used. The 2D free surface elevation measured over the still water level (η) is presented in Dean and Dalrymple (1991) (Eq. 3.43), and the velocity components can easily been obtained from Eq. 3.42. The referenced expressions can be applied explicitly. However, not every variable is known in advance: wave length (L) has been used without being given, and it is obtained by solving iteratively the dispersion relation [Dean and Dalrymple (1991), Eq. 3.36].

For each wave theory analogous expressions to the referenced ones are obtained. The references in which they can be found are

Table 1
Wave generation references.

Theory	Reference	Comments
Stokes I and II	Dean and Dalrymple (1991)	
Stokes V	Skjelbreia and Hendrickson (1960)	
Cnoidal	Svendsen (2006)	Best fit solver. Makes use of ALGLIB open source libraries[a].
Streamfunction	Fenton (1988)	No solver programmed. Its input is the output coefficients from Fenton (1988) programme.
Solitary wave	Lee et al. (1982)	Boussinesq theory.

[a] http://www.alglib.net/.

listed in Table 1, along with some remarkable information about the equation solvers implemented within the boundary condition.

First order directional irregular waves are generated as a linear superposition of Stokes I waves for a given number of components (N), see Eq. (6). This approach is physically correct, as most of the times by discretising a real wave spectrum a large number of components with very small amplitude are obtained. Each of the components is defined by its wave height (H_i), wave period (T_i), wave phase (ψ_i) and the direction of propagation (β_i). Free surface and orbital velocity components are given by:

$$\eta = \sum_{i=1}^{N} \frac{H_i}{2} \cos\left(k_{x\,i}x + k_{y\,i}y - \omega_i t + \psi_i\right). \tag{6}$$

$$\begin{aligned} u &= \textstyle\sum_{i=1}^{N} \frac{H_i}{2}\omega_i \cos^2(\Delta\beta_i) \frac{\cosh[k_i(h+z^*)]}{\sinh(k_i h)} \cos(\theta_i)\cos(\beta_i) \\ v &= \textstyle\sum_{i=1}^{N} \frac{H_i}{2}\omega_i \cos^2(\Delta\beta_i) \frac{\cosh[k_i(h+z^*)]}{\sinh(k_i h)} \cos(\theta_i)\sin(\beta_i) \\ w &= \textstyle\sum_{i=1}^{N} \frac{H_i}{2}\omega_i \cos^2(\Delta\beta_i) \frac{\sinh[k_i(h+z^*)]}{\sinh(k_i h)} \sin(\theta_i) \end{aligned} \tag{7}$$

in which $\Delta\beta_i$ corresponds to the difference between each component direction and the vector normal to the boundary pointing inwards the domain, as shown in Fig. 2. Note that in the three latest equations θ_i stands for the total phase of each component. Regarding the rest of variables: k_x and k_y are the components of the wave number vector, and are obtained projecting it on the horizontal axis: $k_x = k\cos(\beta)$ and $k_y = k\sin(\beta)$. x and y are the coordinates of the given point. h is the water depth. And finally, z^* is the vertical coordinate of the given point in a modified coordinate system for which the origin is located at the initial still water level. This latter feature allows several wave generation patches with different bottom levels.

Despite the directionality, the boundaries are not capable of generating outward ($|\Delta\beta| > \pi/2$) or tangential ($|\Delta\beta| = \pi/2$) waves, so those should be left out. This is taking only angles smaller than $\pi/2$ for each side. For this purpose a classical square cosine function ($f = \cos^2(\Delta\beta)$) has been used. The resultant decreasing factor (f) as a function of the angle difference is shown in Fig. 3. This factor is multiplied by the velocities of each component at the boundary, as presented in Eq. (7), leaving the free surface level unmodified.

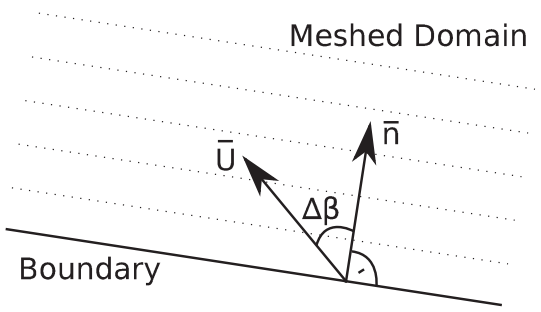

Fig. 2. $\Delta\beta$ definition.

Since with the first order wave generation theory, the group bound wave is not reproduced (Barthel et al., 1983), a correct wave representation needs to include second order effects. Lacking such feature makes spurious free waves to be generated. Therefore long wave effects are underestimated in shallow water and maximised in deep water as stated in Sand (1982). Second order irregular wave generation takes into account the interaction between the individual primary wave components, two by two, and it is built on top of the first order method. Currently, it only supports components travelling in the same direction, therefore $\beta_i = \text{const}$.

In this case, the theory by Longuet-Higgins and Stewart (1960) completed with Baldock et al. (1996) is applied as in Torres-Freyermuth et al. (2010). The reader is referred to such papers for further details, as only a brief description will be given here. The second order effects are added to the first order free surface level and to the velocity. The only new variables introduced are C, D, E and F, which are defined in Longuet-Higgins and Stewart (1960), and depend on the component properties. C and E control the subharmonic generation while D and F generate the superharmonic interaction.

Finally, piston-type wavemaker velocity profile replication is the only theory which has a distinctive behaviour. However, no movement of the boundary is considered. The input is a time series of the wavemaker displacement or velocity, and optionally free surface at the wavemaker. Either way only velocity is used, so if displacements are given, velocity is calculated as a first order forward derivative in time and applied to the total time step. The constant velocity profile as generated by the laboratory wavemaker is applied to the water column.

Additionally, active wave absorption can be activated for wave generating boundary. This feature is explained later on this paper, but as a mere introduction it allows waves reaching the boundary to be absorbed. The result is that the simulation is more stable because the energy and water levels do not increase unboundedly (Fig. 3 in Torres-Freyermuth et al. (2010)), which effectively allows for longer simulations.

3.2. Active wave absorption: theory

Active absorption of waves is one of the key features of physical and numerical experiments in ocean engineering. At prototype scale reflected waves travel away from the study zone. However, in physical or numerical experiments this is not the case, the domains are either constrained in dimensions, such as in wave basins and flumes or

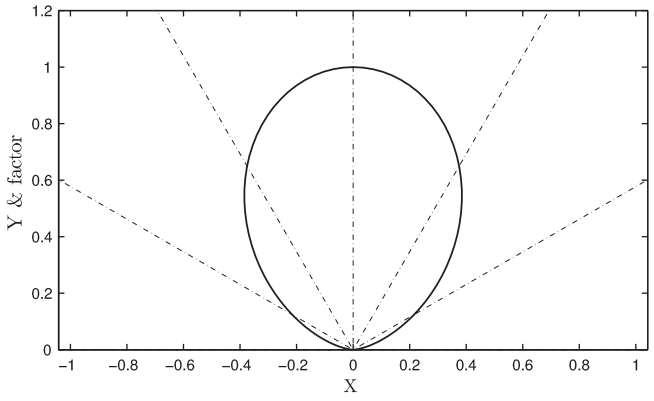

Fig. 3. Square cosine decreasing factor function presented in bold continuous line. The X and Y axes have the same scale in order to evaluate the angle $\Delta\beta$. Only for this figure the angle reference is axis Y. The discontinuous lines are $\Delta\beta$ rays each 30°. The reduction factor is the ordinate of the cut point between the ray and the function. Angles greater than 90°and smaller than −90°have a decreasing factor equal to zero.

cannot be placed at an infinite distance because of computational restrictions. This situation causes inconvenient reflections that, if not handled adequately, could influence the experiment by distorting its results.

The first approach for dissipating the outgoing waves in the past has been using passive wave absorbers. Under this classification we can include dissipative beaches, porous media or porous plates and artificial numerical damping. The absorption achieved is not perfect. For example long waves get reflected even on dissipative beaches, since they do not break, resulting in weakly reflecting BCs. Numerically, passive wave absorbers can be replicated as porous media or as relaxation zones. Practical applications for RANS codes can be found in Pengzhi and Liu (1999), Lara et al. (2006) and for Boussinesq-type models in Wei and Kirby (1995) or Losada et al. (2008).

The second method is active wave absorption. It was first developed for experimental facilities. The system was based on modifying the wavemaker movement based on a measured magnitude (feedback) so that it continues to generate the target wave, while preventing the re-reflection of incoming waves. This system can be applied to numerical models both on wave generation boundaries, but also on pure absorbent ones. In this context, most of the times the boundaries are fixed, as a result wave absorption is achieved by imposing the correct velocity profile on it.

The active wave absorption systems can be divided in three categories: 2D, Quasi-3D and 3D. The details for each one are presented as follows.

3.2.1. 2D absorption

The 2D active absorption method is used as appears in Schäffer and Klopman (2000). It is the easiest technique to be implemented considering the fact that the adjustment for the digital filter is immediate, as it is based on linear shallow water theory. Previous works on other numerical models (Torres-Freyermuth et al., 2010) (Lara et al., 2011) have shown that it works relatively well even when used for waves outside the shallow water range.

It is very convenient to use shallow water theory because the velocity along the water column height is constant, which matches the generation with a piston-type wavemaker. This also makes the evanescent modes not to appear because the velocity profile is the exact one for the progressive wave component. From this wave theory, Eq. (8) can be derived.

$$U\,h = c\eta \tag{8}$$

where U is the horizontal vertically-integrated (uniform) velocity and c is the wave celerity. U is the variable to solve for, and h and η are measurements, consequently there is a need to estimate wave celerity (c). This magnitude is dependent on the relative depth of the waves (kh) in the following way:

$$c = \sqrt{g\,h}\sqrt{\frac{\tanh(kh)}{kh}}. \tag{9}$$

Wave number (k) is very difficult to estimate from measurements, so the practical application of Eq. (9) is achieved by a digital filter assimilation. The use of digital filters for active wave absorption is widely used, for further information refer to Christensen and Frigaard (1994) and Troch and De Rouck (1999). More recently, in Wellens (2012), Eq. (10) is used as a rational approximation to Eq. (9).

$$c^* = \sqrt{g\,h}\frac{a_0 + a_1(kh)^2}{1 + b_1(kh)^2}. \tag{10}$$

A thorough work to adjust a_1 and b_1 coefficients has also been carried out in Wellens (2012). In the present work a decision to leave out these coefficients has been made, understanding that the presented case is the worst scenario and results could be improved with the digital filter coefficients presented in Wellens (2012). Hence, we apply shallow water regime, as explained: $c = \sqrt{g\,h}$, that yields $a_0 = 1$, $a_1 = 0$ and $b_1 = 0$.

In order to cancel out the reflected waves, the boundary must generate a velocity equal to the incident one but in the other direction. Arranging Eq. (8) so that the free surface corresponds to the reflected one η_R (the one to cancel out) leads to the active wave absorption expression presented in Eq. (11).

$$U_c = -\sqrt{\frac{g}{h}}\,\eta_R \tag{11}$$

in which U_c is the correction velocity that is applied to a vector perpendicular to the boundary and pointing into the domain; and the reflected wave height (η_R) is calculated by subtracting the measured elevation at the wavemaker (η_M) from the target one (η_T), according to the expected reflection-free wave generation: $\eta_R = \eta_M - \eta_T$.

This theory was first developed for wave flumes, where the results are usually two dimensional, but can easily be extended to the three dimensions. If reflected waves propagate parallel to the wavemaker the expected behaviour is exactly the same as in the 2D case. If that is not the case the absorption theory can be applied to the individual paddles of the wavemaker independently.

However there is a problem in absorbing in 3D with the 2D theory, as only the wave component perpendicular to the boundary can be absorbed. The other component, which is tangential to the wavemaker, continues to propagate along the boundary until it reaches a lateral dissipative device, if available. Otherwise it will reflect, as a plane wavemaker cannot absorb such a wave, because it can only introduce shear stresses. The influence of the latter wave component perturbs the boundary condition, as presented later.

3.2.2. Quasi-3D absorption

Following the example presented in Schäffer and Klopman (2000) a method to absorb oblique waves is presented. This is only a correction of the already presented 2D absorption theory, enhanced accounting for a known angle of incidence. The practical application is to reduce velocity by a factor $\cos(\Delta\beta)$, as presented in Eq. (12).

$$U_c = -\cos(\Delta\beta)\sqrt{\frac{g}{h}}\,\eta_R \tag{12}$$

Note that when incidence is parallel to the boundary ($\Delta\beta = 0$), absorption velocity remains completely unaffected, since it is a true 2D condition. As waves approach the parallel direction, the theory is expected to underperform, never being able to absorb the tangential component of the wave as $\Delta\beta$ approaches 90°. This will finally lead to a stationary wave along the wavemaker if the situation is not handled correctly.

This method was developed for piston wavemakers, but it is modified here taking advantage of the numerical model capabilities, to obtain better performance. Instead of reducing the correction velocity and applying it to the perpendicular direction to the boundary, the correction velocity is still the one calculated with Eq. (11), but this time it is applied to the desired direction. Generally, this new approach is able to absorb better than projecting the velocity and allowing the tangential component to flow along the boundary.

The performance of this boundary condition is outstanding but there is a clear drawback: most of the times the direction of the incident waves cannot be anticipated, or radiation from the structure makes that direction to change either in time or along the boundary extents. Nevertheless good performance is expected even for small deviations in the direction of the absorption Schäffer and Klopman (2000).

3.2.3. 3D absorption

Although both the 2D and Quasi-3D absorption theories can be used to absorb with reasonable results in 3D cases, a specific full 3D theory is needed to obtain lower reflection coefficients or to avoid wave radiation from the absorbing boundaries. The distinctive element of this method is that it uses the feedback additionally to evaluate wave directionality.

The following method is original and quite simple, furthermore it needs no tuning, but due to the complexity of measurements needed, it can only be applied to numerical models. Traditional 3D absorption theories for laboratory wavemakers rely on measuring free surface in front of the individual paddles and by calculating the derivatives or applying a digital filter to this data the directionality is measured. This involves interconnection between wave paddles. Our method eliminates the error introduced by the discrete calculation of derivatives, acting for each paddle independently.

As the aforementioned methods, this one is also based in shallow water wave theory, i.e. such waves have a velocity field which is constant along the whole water column. As a result, averaging the horizontal components of velocity all over the water depth will theoretically yield the same value as in each point of a vertical line. The same principle is applied to the direction of the horizontal velocity.

The practical application involves the calculation of a mean horizontal velocity with its mean direction for each vertical slice of the boundary. This velocity can be decomposed in two independent components: one normal to the paddle and another tangential to it. Also the measured free surface level at that vertical slice is needed. Wave directionality cannot be inferred using these two components of velocity at the same time, since absorbing waves involves imposing a certain velocity on the boundary, which will completely distort the measurements. Hence, correction velocity can only be prescribed on the perpendicular direction to the paddle, as in the usual wave absorption theories using piston wavemakers, leaving the other component unmodified so that it can be measured. The implementation is presented graphically in Fig. 4.

By simple calculations wave directionality can then be obtained, as follows:

$$|U_{calc}| = \sqrt{\frac{g}{h}}\,\eta_R. \tag{13}$$

$|U_{calc}|$ is the total expected modulus of velocity, based on the measured free surface level minus the expected one (still water level). By decomposing it into the two horizontal components it is obvious that:

$$U_{calc}^2 = U_{corr}^2 + U_{tg}^2. \tag{14}$$

in which everything is known except for U_{corr}, the correction velocity that has to be applied in the perpendicular direction to the paddle in order to absorb the waves. To solve for U_{corr} modulus, the square root of a subtraction must be obtained:

$$U_{corr} = \sqrt{U_{calc}^2 - U_{tg}^2}. \tag{15}$$

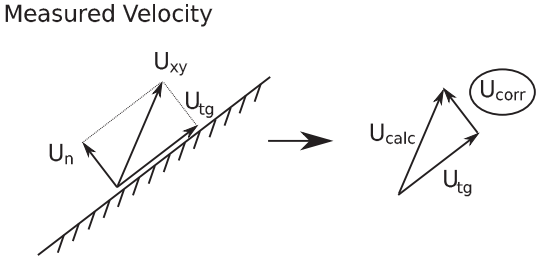

Fig. 4. Scheme for the full 3D absorption theory.

It is easy to notice that when the tangential component of the velocity (U_{tg}) is greater than the total one (U_{calc}) there will be no real solution. To account for it the value inside the square root is evaluated and if it is negative it is set to zero, and no absorption is taking place.

Once again the problem of having a wave which propagates along the wavemaker is present. There are also two main problems related with corners. The first one is dealing with this tangential wave component which cannot be absorbed along the wave maker. The second is that if we had a 90°corner for two absorbing boundaries, the perpendicular component for the first will be the tangential one for the second and vice versa. This causes a stability problem because wave directionality cannot be correctly estimated. A single solution solves all these problems. This is to choose a number of paddles (user-defined vertical slices of patch, which resemble the individual paddles of a wavemaker) near the edges only capable of extracting water according to Eq. (11). The reason to limit in-flux of water in such parts is because in the case of an acute corner, water is pushed directly into a small space, making the level to increase very rapidly, and most of the times reaching the top of the mesh, which will lead to loss of mass in that zone.

3.3. Wave generation: implementation

The numerical implementation is common for all the wave theories. Only a small change is made in the case of the piston-type wavemaker replication when no free surface is provided. The current approach takes into account three types of cells: wet cells, which have all the vertices below the free surface level; dry cells, which have all the vertices above the free surface level; and partial cells, in which free surface is between the lowest and highest vertices of the cell.

Wave generation involves setting the values of velocity and VOF function (field “alpha1”, α_1 from now on), therefore their implementation is separate, but they share most of the source code. Pressure is not set directly, it is calculated using the “buoyantPressure” boundary condition. This special function available in OpenFOAM® calculates the normal gradient from the local density gradient. This ensures that the second derivative of pressure in the orthogonal direction to the boundary is zero.

During the first time step of the model, and only then, several processes are carried out. Wave generation variables are read and relevant variables are calculated using wave theory. Also the initial still water depth at the patch is measured, as the wet area of the patch (sum of the individual face areas times α_1 of the owner cell) over the total patch area.

For the piston-type wavemaker replication, if free surface is not provided, the corresponding constant velocity profile along the whole water column is applied. This is done by multiplying such velocity times α_1 in each cell, in order not to introduce air velocity. No further considerations are made. If the free surface elevation is provided, it is interpolated linearly in time and the procedure is as the general one, which is explained next.

For the rest of the cases presented, an expression to calculate the free surface is provided by the correspondent wave theory. Consequently, at each time step, the theoretical and measured free surface levels can be compared in order to trigger active wave absorption. The following method takes into account the possibility of high amplitude reflected waves reaching the generation patch, and makes the simulation more stable.

In the next lines “zero gradient” is used to indicate that the boundary face value is set to the value of its owner cell or mathematically for any variable q: $\frac{\partial q}{\partial n} = 0$, where n is the normal direction to the face. Please, note that it does not refer to “zeroGradient” OpenFOAM® built in BC.

There are three different areas, which are indicated in Fig. 5, depending on whether the measured level is higher than the theoretical one (positive reflected wave, left panel on the figure) or lower

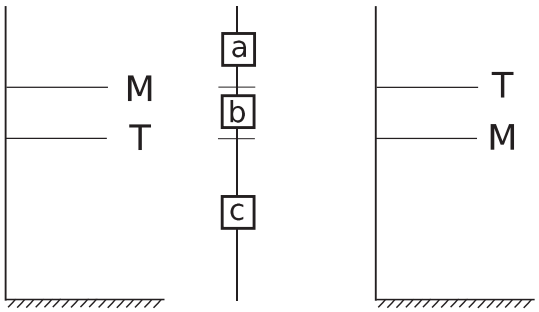

Fig. 5. Water level in a wave generating patch. "*M*" stands for measured value, "*T*" stands for theoretical value. Three zones (a, b and c) and two interfaces are present in each case.

(negative reflected wave, right panel). This disposition provides three different areas ("a", "b" and "c") and two interfaces between them. The implementation is explained next, and can be summarised as shown in Table 2.

Zone "a" is common in both cases, and corresponds to air ($\alpha_1 = 0$). Therefore, the faces within it have α_1 and velocity set to zero.

The interface between "a" and "b" is different depending on the case, because wave velocity is set only below the theoretical level. When $M > T$ carries a zero gradient value for α_1 and zero to velocity. If $T > M$, an especial procedure is performed. The intersection between the theoretical water level and the cell is calculated to obtain the corresponding α_1 of the cell. Also the centroid of the cell wet part is obtained to calculate the velocity in that point. Velocity is set as the multiplication of both quantities. This is done to prevent spurious air velocities in the interface, which tend to lower the Courant number and to lower stability.

Zone "b" also depends on the case. When $M > T$, α_1 is set to zero gradient and velocity is directly zero. When T > M, α_1 is set to one when water flux is inwards and to zero gradient otherwise. Velocity is set to the theoretical value. This sometimes may cause water droplets to appear in the boundary, especially when the reflected amplitude is large (in the order of several cells).

The interface between "b" and "c" sometimes has water above ($M > T$) and sometimes should ($T > M$), but due to the reflected waves it does not. This condition changes its behaviour depending on it, as shown in Table 2 (left vs. right table). In the first case, α_1 is set to zero gradient, and the velocity is calculated in the same way as in zone "a–b" for $T > M$, for the same reasons explained above. In the second case if water is flowing in, it is set to one, and to zero gradient otherwise. Velocity in this case is set to the calculated value.

Finally, the zone "c" is also common to both cases, as it is always under the measured and theoretical values, therefore it corresponds to water ($\alpha_1 = 1$). If the flow is entering the domain, α_1 on the face is set to one, otherwise it is set to zero gradient. This configuration is more stable than setting it always to one, as it has been observed that this other solution can more easily cause α_1 to reach negative values despite the fact that the "MULES" solver ensures boundedness between zero and one. Velocities are set to the theoretical value.

When an interface coincides with a cell, that cell is automatically an interface cell. Should both of the mentioned interfaces coincide within a cell (e.g. small reflected waves or even $T = M$), the priority of the cell is from below to the top, from "c" to "a".

The velocity and α_1 can be set in different ways, as decided by the user. First and the most obvious way is face by face. Each of them owns a cell which is formed by a number of points, and by a centroid, all of them having different coordinates. The belonging zone of the face ("a"–"c") is checked using the highest and lowest points of the cell in the *Z* direction, while velocity is calculated using the centroid coordinate of the face. This boundary condition also supports an automatic division of the generating patch in vertical slices. Such zones resemble the disposition of individual paddles within a wavemaker, and behave in the precise way to allow closer replication of such device without the inconvenience of having to manually divide the boundary in advance. Cells within each of these zones lose their *x* and *y* coordinates in favour of the centroid of the paddle, but maintain their height, for α_1 and velocity calculation.

Additionally, if active absorption is connected, the face velocities get corrected adding the calculated value to the ones above, in the way explained in the following section.

3.4. Active wave absorption: implementation

The implementation of pure active wave absorption is easier, as there is only need to prescribe the velocities. Pressure boundary condition is set to "buoyantPressure" again, and α_1 to "zeroGradient".

The practical application of the absorption theory consists in dividing the boundary in a given number of vertical elements. The minimum is one, case in which the whole boundary will absorb globally. For each of the individual elements the initial still water level is calculated and saved. Then each time step the actual water level at each paddle is obtained and the correction velocity is calculated according to the previous theories e.g. using Eq. (11) for 2D.

The correction velocity is then recalculated cell by cell, multiplying the obtained value (checking the paddle in which it is included) by the value of α_1 in that cell. This is done to prevent the propagation of air pockets close to the boundary. The resultant velocity is applied in the perpendicular direction to the face (for 2D and full 3D absorption) or to the given direction (Quasi-3D). If such velocity is positive (in-flux), only the cells below the measured ("*M*") water level are given this value, the rest are set to zero. Otherwise (out-flux) all the cells are set to the recalculated velocity value. The main reason to do this is to gain stability, as if a water droplet from a splash was higher than the water level on the patch it will not propagate when water is flowing into the domain, and it will flow out otherwise.

4. Validation

Several cases have been simulated in order to test the model wave generation capabilities and the efficiency of the active absorption BCs implemented. First, the 2D absorption theory will be tested in 2D cases for solitary and regular waves. Then all the theories will be tested in 3D cases with oblique incidence of solitary waves. Finally an irregular wave case is analysed.

All the cases in the present paper have been tested using a $\kappa-\varepsilon$ formulation to model turbulence, as it is widely used. However, the results seem to be unaffected by it, as expected. This is because the examples shown are not highly influenced by turbulence, as there is no wave breaking. Both $\kappa-\varepsilon$ and $\kappa-\omega$ SST models have been considered in the companion paper (Higuera et al., in press).

In the following cases other boundary conditions have also been used. The walls and floor are set to no slip boundary conditions for velocity, "zeroGradient" for α_1, "buoyantPressure" for pressure and

Table 2
Overview of the boundary condition values depending on the zones established in Fig. 5.

	$M > T$		$T > M$	
	α_1	U	α_1	U
a	0	0	0	0
a–b	$\frac{\partial \alpha_1}{\partial_n} = 0$	0	α_{1calc}	$U \cdot \alpha_{1calc}$
b	$\frac{\partial \alpha_1}{\partial_n} = 0$	0	In $\rightarrow 1$ Out $\rightarrow \frac{\partial \alpha_1}{\partial_n} = 0$	U
b–c	$\frac{\partial \alpha_1}{\partial_n} = 0$	$U \cdot \alpha_{1calc}$	In $\rightarrow 1$ Out $\rightarrow \frac{\partial \alpha_1}{\partial_n} = 0$	U
c	In $\rightarrow 1$ Out $\rightarrow \frac{\partial \alpha_1}{\partial_n} = 0$	U	In $\rightarrow 1$ Out $\rightarrow \frac{\partial \alpha_1}{\partial_n} = 0$	U

special wall functions for κ, ε or ω. The top boundary has a special condition for α_1 named "inletOutlet", which allows water to flow out and air to flow into the domain when needed, as driven by the fixed total pressure value specified; velocity is also calculated to satisfy the pressure condition; turbulent variables are also set to "inletOutlet", specifying the in value. Finally, the wave generating boundary acts as an open condition for turbulent variables, being set to "zeroGradient".

4.1. 2D absorption of a solitary wave in a wave flume

All the 2D cases have been simulated using the same mesh, which is 20.62 m long, 0.58 m wide and 0.70 m high. The spatial resolution chosen is 2 cm on the horizontal direction and 1 cm on the vertical one, which makes a fully structured and orthogonal mesh of 1031×70 cells.

The first tests were carried out by generating a solitary wave and absorbing it at the opposite end. Two wave heights were considered: 5 cm and 15 cm, both using Boussinesq theory. Water level is set at 0.40 m. A unique wave gauge is located 7.50 m away from the wavemaker and measures water elevation at 20 Hz. The schematic view of the flume is presented in Fig. 6. Reflection coefficient is estimated as the quotient between the reflected wave and the initial wave at the gauge. As the reflected wave has to travel one way and back its total displacement from the gauge is 26.24 m. Estimating a long wave celerity $\left(c = \sqrt{gh}\right)$ the wave travels at approximately 2 m/s, so reflections are expected about 13 s from the first pass. Nevertheless 60 s are simulated in order to check also the stability of the boundary condition when water is still. As the mesh is quite small (70,000 cells), it runs on 1 processor (2.93 GHz), simulating the full 60 s in 1 h and 30 min.

The results of the free surface level are shown in Fig. 7. At the top panel the free surface level at the only free surface gauge is presented. The lower panel shows the spatial and temporal variation of free surface level along the flume. The X axis corresponds to the length of the flume, while the vertical axis includes both space and time. Each line represents the free surface along the flume for a given time, every 0.10 s. The baseline for each one is placed at the time of the snapshot, and from it the free surface is represented in the same axis, but amplified by a factor of ten. From the end point of the figures until second 60, water shows smaller oscillations than the ones caused by the first reflection. The small oscillations which follow the soliton are an artificial effect of the wave generation boundary condition, and are generated as the solitary wave gains a stable profile, getting rid of several components.

For $H = 0.05$ m, the peak of the solitary wave reaches the wave gauge at time = 6.40 s with a height = 0.0461 m. The biggest reflected wave is 0.0007 m in height and it reaches the gauge at $T = 20.80$ s. The reflection coefficient for the 5 cm wave is then 1.51%.

For the largest wave height case, the peak of the solitary wave reaches the wave gauge at time = 4.70 s with a height = 0.1594 m. The largest reflected wave is 0.0042 m in height and it reaches the gauge at $T = 18.55$ s. The reflection coefficient for the 15 cm wave is then 2.63%.

In both cases the reflected wave is so small that it lies in the subgrid scale. The long time simulated proves the stability of the boundary condition for very small free surface disturbances.

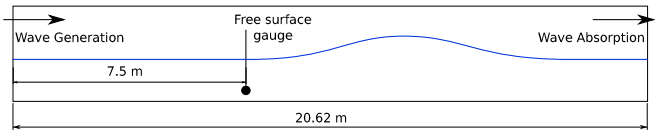

Fig. 6. Schematic view of the 2D flume.

4.2. 2D absorption of regular waves in a wave flume

These tests of regular waves in a flume have been simulated using the same 2D mesh as for the solitary waves. Six cases have been considered, as a combination of two wave heights: 5 cm and 15 cm; and three different wave periods: 2 s, 3 s and 4 s. Still water level is set at 0.40 m again. The case $T = 2$ s, $H = 5$ cm is generated using Stokes I theory, $T = 3$ s, $H = 5$ cm is generated with Stokes II and the rest of the cases with cnoidal theory. All of them have simultaneous generation and active wave absorption connected apart from the active wave absorption on the other end.

This time there is a need for at least 3 gauges to accurately estimate the reflection of the boundary. Following Mansard and Funke (1980) methodology, the distances between the gauges are calculated based on the wave length in order to obtain a stable solution. The first gauge is always placed at 7.50 m. The distance between the first and second gauges is fixed: $X_{12} = \frac{L}{10}$. The distance between the first and third one is bounded: $\frac{L}{6} < X_{13} < \frac{L}{3}$ while $X_{13} \neq \frac{L}{5}$ and $X_{13} \neq \frac{3L}{10}$. To fulfil these restrictions, $X_{13} = \frac{L}{4}$ has been chosen. For each of the wave periods there is an associated wave length, calculated using the dispersion relationship. In Table 3 wave lengths and distance between gauges for each wave period are given.

All the cases have been simulated for 120 s using 1 core (2.93 GHz). The mean elapsed time is greater than double, compared with the previous case, as larger velocities inherent to the waves are present throughout all the simulation. The simulations were completed in less than 4 h.

The reflection analysis is carried out using waveLab® 3 software, using the signal of the 3 gauges as input, and eliminating the first 5 waves to start with a more or less steady state. The calculations of Mansard and Funke (1980) plus an inverse FFT in order to obtain the reflection coefficients in both the frequency and temporal domains are carried out. The reflection results can be seen in Table 4. Incident (regular continuous line) and reflected (bold continuous line) time signals for $T = 2$ s, $H = 15$ cm and $T = 4$ s, $H = 5$ cm cases, are presented in Fig. 8. The instantaneous reflection coefficient (dashed line) can also be seen.

The performance of this boundary condition is very good, leading to reflection coefficients under or about 10% for the typical range of wave periods and heights on flumes. As expected, when period grows the reflected waves decrease because waves are closer to the initial assumption: shallow water waves. For waves with smaller periods worse performance is expected. For higher periods the reflection coefficient will continue to decrease until the waves reach the shallow water condition. Following the work by Wellens (2012), explained in Eq. (10), will contribute to obtain a more even behaviour and better results along all the range of relative water depths. Nevertheless, this is not the goal of the current study.

4.3. 3D absorption of a solitary wave in a wave tank

Oblique incidence is obtained by setting up a special domain instead of generating obliquely, which can also be done. The wave tank has a geometry controlled by the angle of incidence (θ), while the dimensions specified in the right panel of Fig. 9 and the height (0.70 m) are fixed. The mesh is generated using the "blockMesh" utility, with the same parameters independently of angle θ: 125 cells in the X and Y directions and 40 cells on the vertical one. The resulting mesh has 625,000 cells and is structured but not always orthogonal. Resolution is dependent on θ. For the case of $\theta = 0$ the horizontal resolution is 4 cm and the vertical one is 1.75 cm. For all the cases tested using this mesh, nine free surface gauges have been placed. Their location and number are shown on the left panel of Fig. 9, and coordinates can be obtained as all the combinations for X and Y with values 1.25, 2.5 and 3.75 m. For reference, waves are always

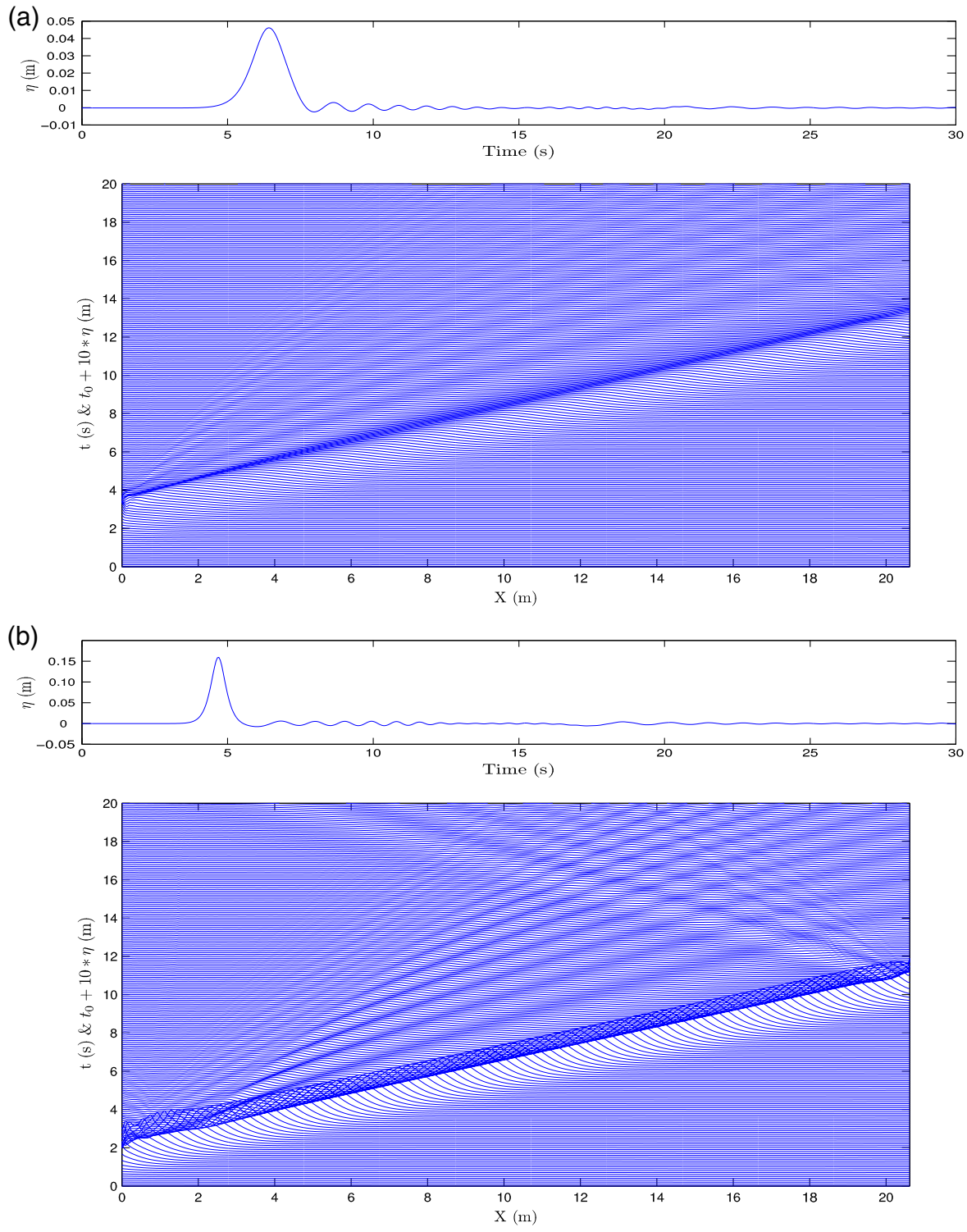

Fig. 7. Solitary wave on a 2D flume with a 2D absorbent end: free surface at the gauge and spatial/temporal evolution. (a) $H = 5$ cm. (b) $H = 15$ cm.

Table 3
Regular waves in a 2D flume: wave lengths.

T	L	X_{12}	X_{13}
2 s	3.70 m	0.370 m	0.924 m
3 s	5.77 m	0.577 m	1.441 m
4 s	7.79 m	0.779 m	1.948 m

Table 4
Regular waves in a 2D flume: reflection analysis given by waveLab® 3.

T	H	
	5 cm	15 cm
2 s	4.6%	11.2%
3 s	3.8%	7.3%
4 s	2.3%	6.7%

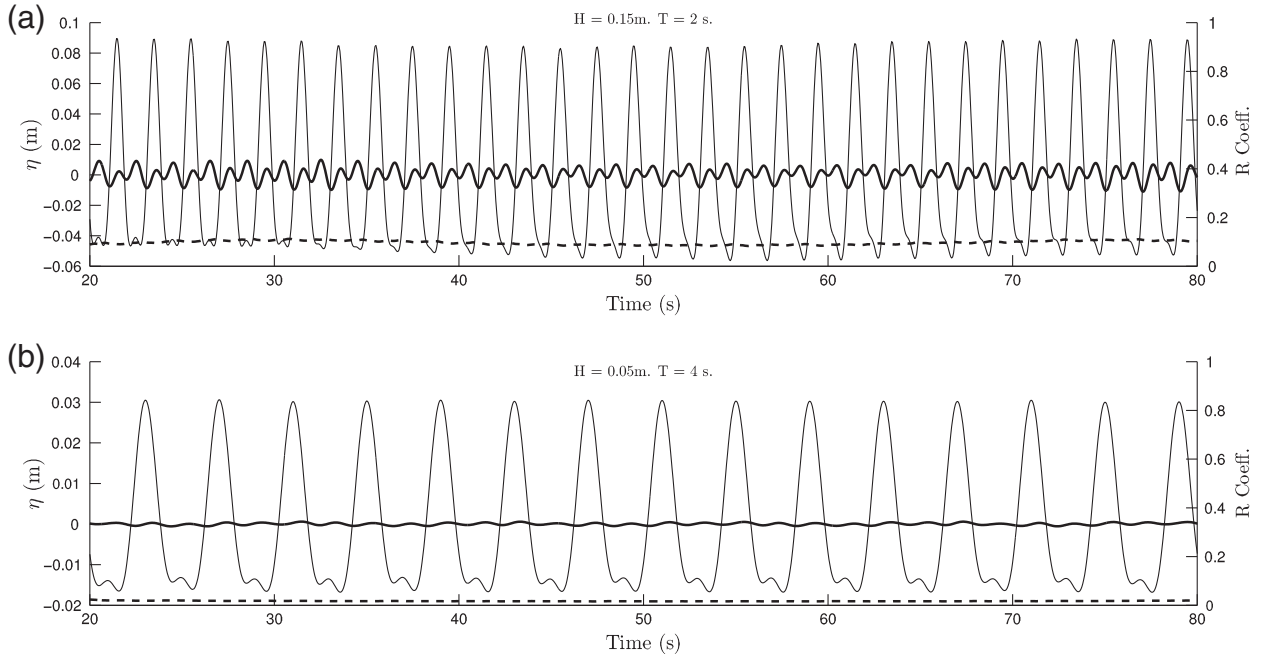

Fig. 8. Reflection analysis of regular waves in a 2D flume for 2D absorption in the end. Wave characteristics are given below each panel. The regular continuous line is the incident component, the bold continuous line is the reflected component, both of them having the vertical scale on the left side. The dashed line is instantaneous reflection coefficient and its scale is on the right. (a) $T=2$ s, $H=15$ cm. (b) $T=4$ s, $H=5$ cm.

generated on plane $Y=0$, so they propagate towards the positive values of X axis.

4.3.1. 0° incidence angle, absorbent end

The first test is the 3D simulation of the 2D solitary wave case, with normal incidence ($\theta=0°$). The tank is 5 by 5 m. The solitary wave is 15 cm in height and simultaneous active wave generation and absorption is active. The boundary opposite to wave generation is absorbent, and it is automatically divided into 25 individual paddles, each of which is 5 cells wide and evaluates water level and corrected velocity independently. The lateral walls are set to no slip boundary condition. The case runs on 2 cores (2.93 GHz), and completes 10 s of simulation in 1 h and 30 min.

The free surface elevation at the 3 first gauges is shown in Fig. 10. Only those gauges are presented because this is virtually a 2D case, as running a 3D version of it does not introduce relevant changes, since there is no wave breaking. It can be seen that the first gauge (top panel), which is the closest to the generation boundary shows a wave with certain skewness due to local effects. In the next gauge (middle panel) the wave shape has a regular profile. The reflected wave is of the same order of the perturbations that follow the soliton, and cannot be clearly seen. Nevertheless it can be measured, and the resulting reflection coefficient for the central gauge (number 5) is 4.39%.

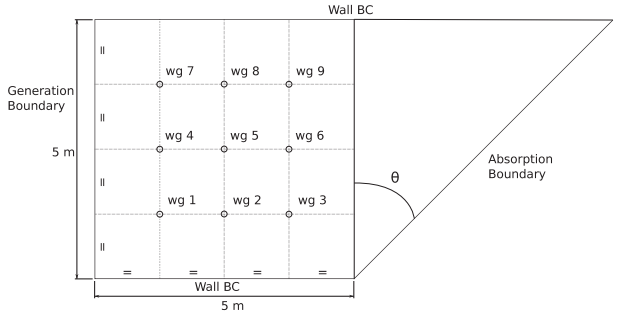

Fig. 9. Geometry and wave gauges of the 3D wave tank. The figure is an application for $\theta=45°$.

The solution for the Quasi-3D case is identical, as the solitary wave propagates parallel to the paddle. The results for the full 3D case are also virtually the same as the case in 2D, since no velocities are expected to develop in the direction of the paddle, therefore the resulting reflection coefficient for the central gauge is 4.13%. Both of them are very close. However, the reflection coefficients are almost double compared with the value that was obtained in the 2D case. There are several reasons that explain this behaviour. First, the tank domain is not as long as the flume and the free surface gauge is not located at the same relative location. Secondly, the discretisation is different, as the flume cells are almost half in size with respect to the ones in the tank.

4.3.2. 0° incidence angle, full absorbent walls

This case is identical to the previous one, but the lateral walls and the end are set to absorbing boundaries with the same parameters as before (i.e. 25 individual paddles). Only 2D and full 3D absorption methods can be used, as Quasi-3D would introduce only shear stresses on the lateral faces. As it has already been mentioned, it is impossible to absorb a wave which propagates along a boundary. The ideal behaviour for the lateral boundaries will be to actually behave like walls, hence the results will match those of the previous case. The 2D absorption theory calculates the velocity only measuring water levels, as a result it will take water out when the wave crest passes and make it flow in when the wave trough arrives. The full 3D version is expected to reduce this effect. The purpose of this test is to evaluate the magnitude of these waves that get radiated from the lateral boundaries.

In Fig. 11, a cross comparison between the 2D theory (dashed line) and the full 3D one (continuous line) is presented. It is clearly noticeable that the lateral boundaries disturb the wave in the first case, because as the wave propagates, water is taken out of the domain. Wave height decreases significantly and the smaller troughs that follow the principal wave get maximised, especially along the centre line (gauges 4–6) because the addition of the perturbations of both sides. Some of the differences between the gauges are up to 4 cm,

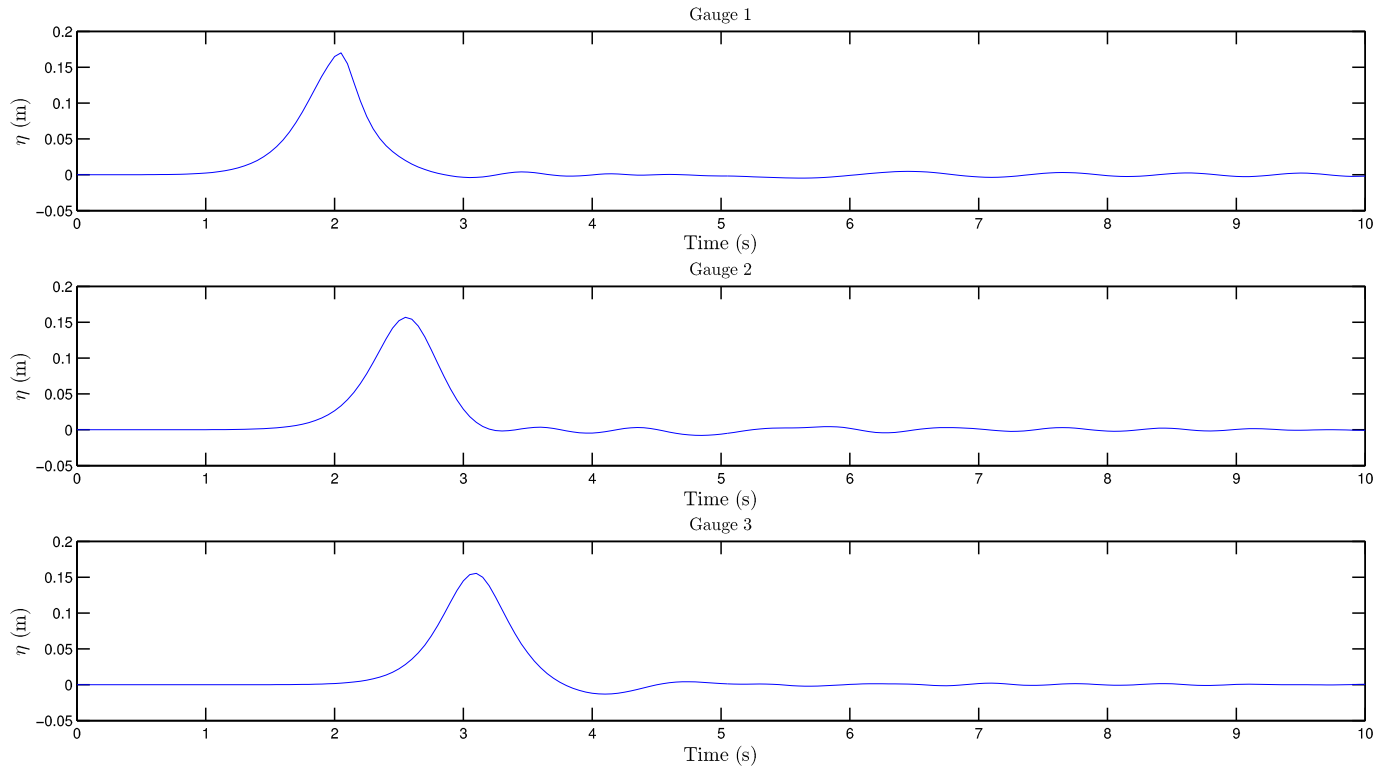

Fig. 10. Free surface gauges for a solitary wave on a 3D tank with a 2D absorbent end. Incidence angle is 0°. The solution is fully 2D, so gauges 4–6 and 7–9 are the same as these.

more or less around 25% of wave height value. Solution continues to be symmetrical in both cases. The 3D theory (continuous line) can be assimilated as the reference case, because only differences of 3 mm at most appear compared with the absorbent end case. If both cases were plotted in the graph, they would lie one on top of the other. Nevertheless those 3 mm increase the reflection coefficient by a 2%; namely 6.30%.

We can conclude that the 2D boundary condition is not suitable for 90°incidence as it generates great disturbances, while the developed full 3D theory deals correctly with such a situation.

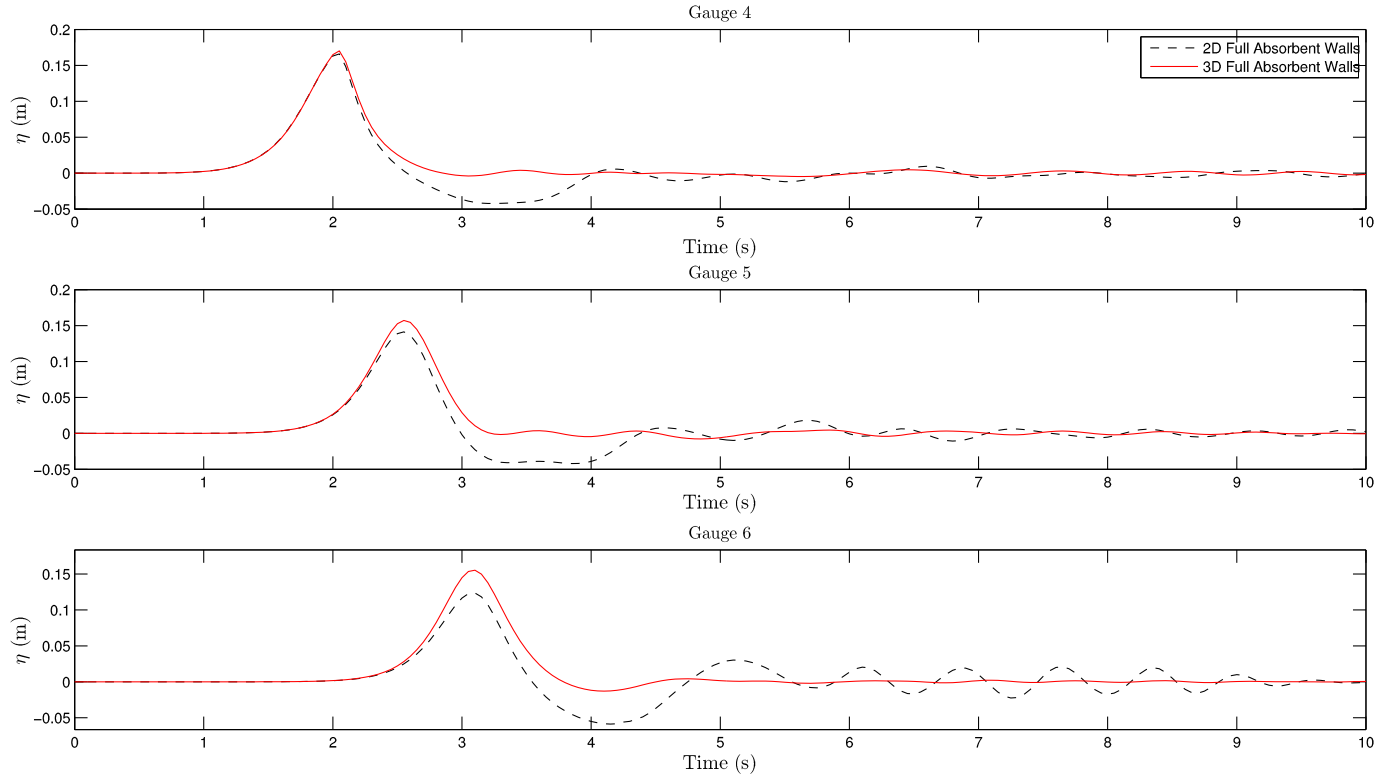

Fig. 11. Comparison of free surface gauges between the solitary wave on a 3D tank with all 2D absorbent walls (dashed line) and all 3D absorbent walls (continuous line).

4.3.3. 45° incidence angle

The mesh is exactly as shown in Fig. 9. The results for the 6 first gauges for all the absorption theories are shown in Fig. 12. For this case reflection is evident and three-dimensional, as the first triplet of gauges shows different reflected amplitudes between them and between the second triplet.

For 2D theory, and in order to avoid stability problems due to the corners, one paddle at the acute end of the boundary is limited to out flux only. The reflection coefficient evaluated on gauge 5 results 7.65%. On gauge 3, towards the end of the series several re-reflected waves can be observed. They are created by the tangential wave component which gets reflected on the lateral walls because those are not absorbent. Performance is not as good as in the previous case where $\theta = 0°$ due to the tangential velocity component, but it is still very low.

Quasi-3D theory shows an outstanding performance, as reflected waves are barely noticeable. The reflection coefficient on gauge 5 is 4.09%, which is almost half compared with the one obtained using

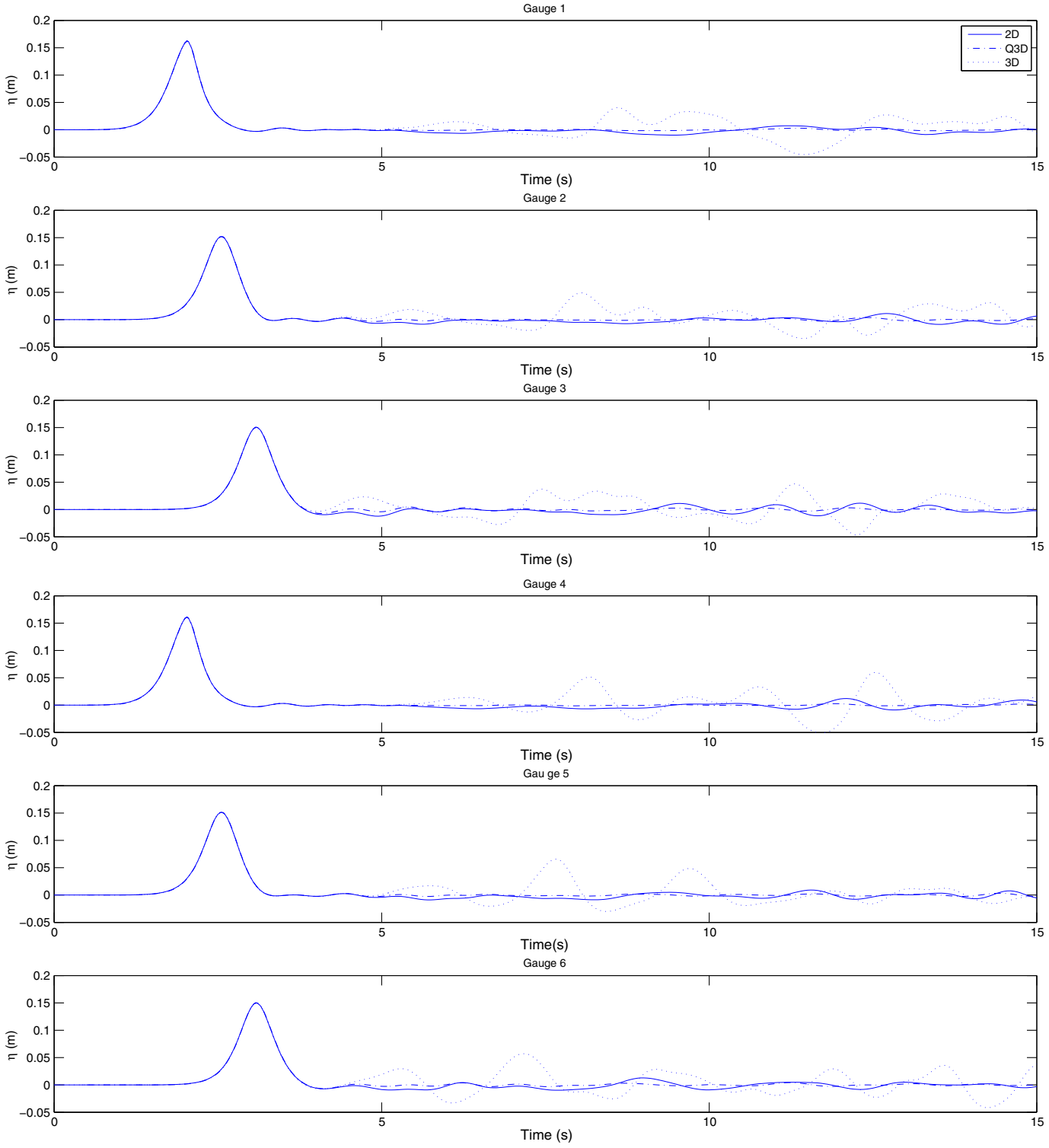

Fig. 12. Free surface gauges for a solitary wave on a 3D tank with an absorbent end. Incidence angle is 45°. Comparison between all the theories.

2D absorption and virtually the same as in the previously studied normal incidence case.

Full 3D theory shows the worst performance amongst all of them, with a reflection coefficient on gauge 5 of 20.63%. In this case all the walls are absorbent to dissipate the tangential component of the wave and one paddle at the acute end of the boundary is limited to out flux only for each of the patches.

4.3.4. 60° incidence angle

The last case is identical, but this time the incidence angle is set to 60°. Once again the behaviour is fully 3D. The reflection coefficients for gauge 5 are: for 2D, 3.64%; Quasi-3D shows the best performance once again with 2.58%; and full 3D reaches 13.92%.

The evolution of this case for the 2D absorption theory is presented in Fig. 13. As the wave starts to flow along the absorbent end, small waves start to be radiated, but the goal to absorb the main wave is achieved, as there is no trace of the original wave. However, the spurious waves reach the longest lateral wall (see time 7.55 s) and then reflect towards the absorbent boundary again, were eventually they are dissipated.

4.4. 3D absorption of directional irregular waves in a wave tank

Realistic sea states have little resemblance with the cases shown above. The real sea state can be described by means of a spectrum, which once discretised can be translated in terms of wave components with wave height, period, phase and direction of propagation.

The synthetic spectrum that has been created includes the typical features of a combined sea state of a sea and a swell states, as it can be seen in Fig. 14a. The mean direction for both portions of it is 45°. The sea has a peak period of 1.5 s, while the swell presents a higher one, 5 s. Both of them have the same significant wave height, equal to 10 cm.

The mesh for this case is the same as for the 45°incidence wave tank. The waves corresponding to the theoretical spectrum are generated in the usual boundary using the newly-generated condition, featuring simultaneous active wave absorption. The rest of the vertical walls are set to fully 3D absorbent boundaries. No other absorption theories have been tested, since 2D absorption will highly radiate waves from the lateral boundaries. A similar case occurs for Quasi-3D absorption, the main direction of the generated waves coincides with the end wall, so if absorption direction is to be set it would create a problem because it would be tangent to the wall. It is very difficult to estimate an incidence angle for the walls in advance.

The case is simulated for a total of 180 s (approximately 100 waves). Completing the simulation takes 9 days in 8 cores (2.93 GHz). Free surface is sampled at 20 Hz. The numerical gauges are placed, following the indications of the seven elements irregularly spaced array in Young (1994). Its central location is gauge number 5 in Fig. 9, and is chosen because it lies in the limit of the shadow zone of the spectrum. The 7 resultant signals are then analysed using waveLab® 3 built-in Bayesian Directional Spectrum Estimation Method (BDM). The resultant directional-frequency spectrum is shown in Fig. 14b. Also free surface in the tank is presented in Fig. 15.

The comparison between both spectra is shown in Fig. 14. The top figure shows the theoretical spectrum and the bottom one is the measured one.

The total energy of the theoretical spectrum (volume under the surface) is equal to $6.2316\times10^{4}\,m^{2}\,rad$. The measured energetic level is a 30% lower, totalling $4.3615\times10^{4}\,m^{2}\,rad$. This decrease of energy is caused by the chosen spectrum and point location, as the components beyond the 45° angle only reach it diffracted. This also makes the energy to be more confined towards 0° direction, reducing the directional dispersion. At the same time, the frequency dispersion from the captured signal increases for the swell state and decreases for the sea state. Another remarkable fact is that the peaks of the sea and swell are correctly represented in frequency and direction, although the measured spectrum is more peaked, as it can be seen in Table 5. This means that the measured spectrum has higher and more pointed peaks, but less broad, as the total amount of energy is lower. The swell state is better reproduced, as the peak direction shows less deviation.

The snapshots in Fig. 15 show the evolution along 5 s of the waves in the tank. it can easily be appreciated that this is a short crested sea state, as no continuous wave fronts are present. Wave obliquity in the generation boundary can be seen in the last two snapshots. The correct behaviour of the absorbent end can also be observed comparing these two frames, especially at the acute end of the tank.

5. Conclusions

In this paper, OpenFOAM®, a free, open source and multipurpose CFD code, consolidated, widely used and rapidly extending, is upgraded to deal with applications in coastal engineering. It lacked a coupled active wave generation–absorption system, which impeded

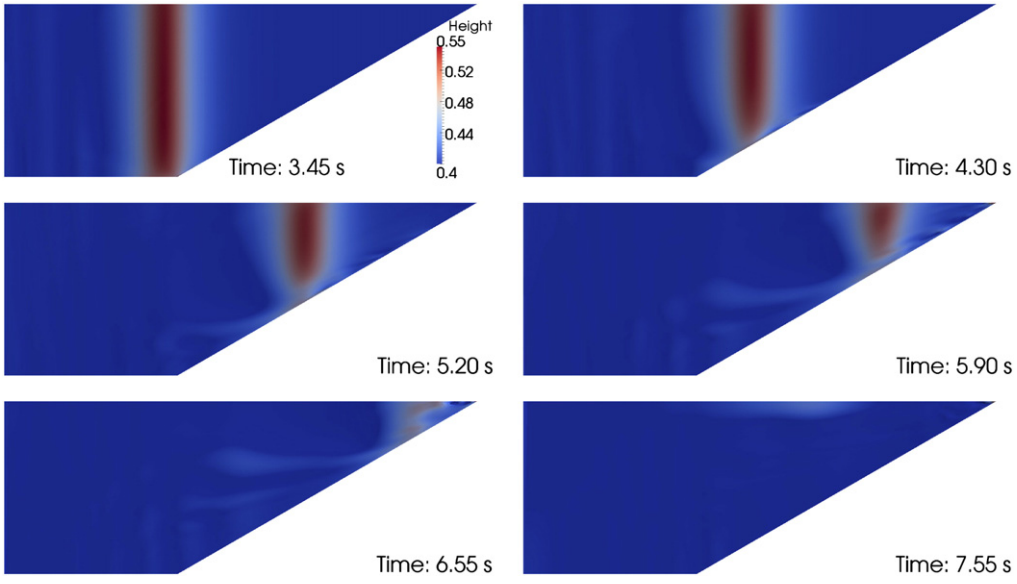

Fig. 13. Free surface for the solitary wave on a 3D tank with a 2D absorbent end. Incidence angle is 60°.

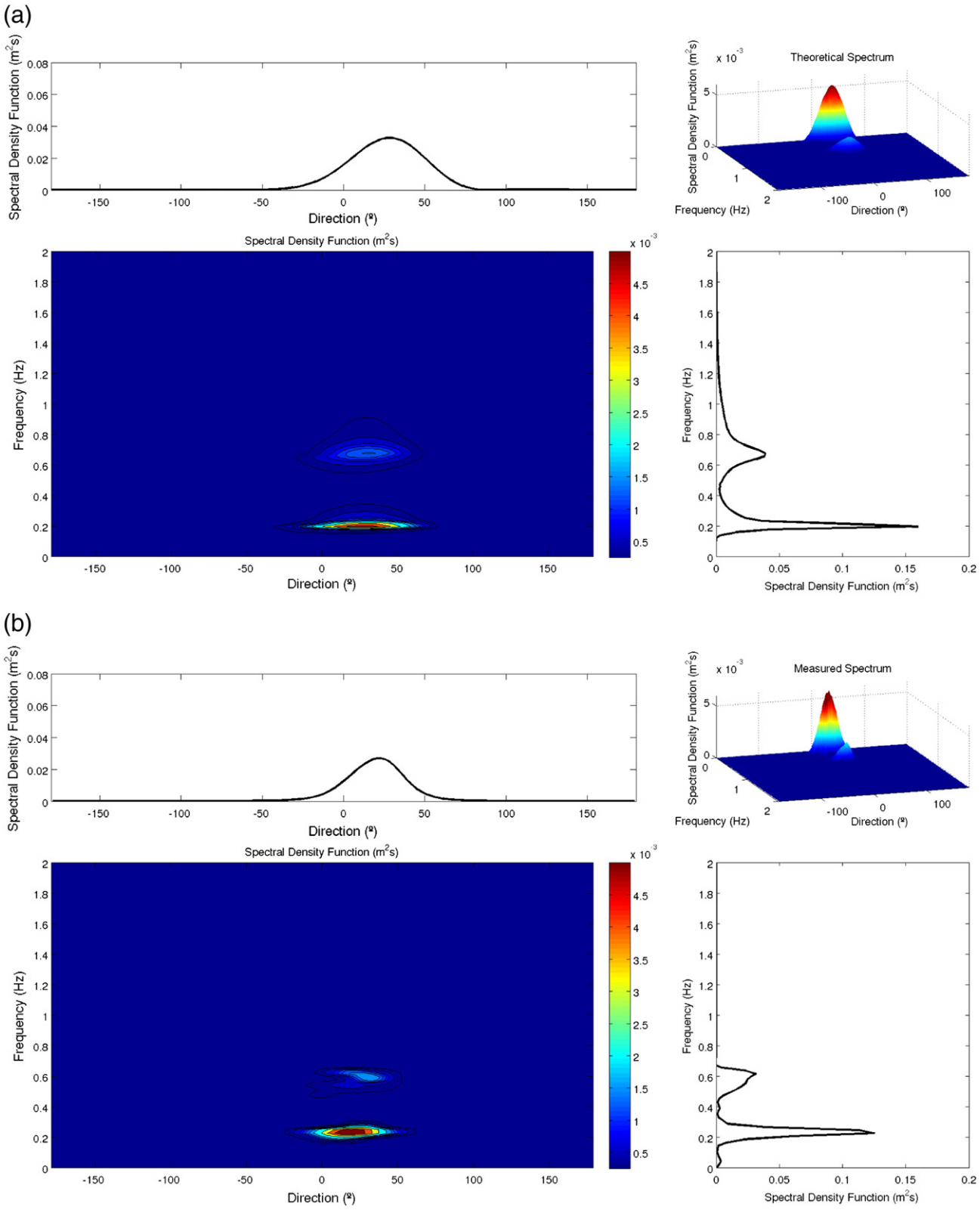

Fig. 14. Theoretical vs. measured spectra of the irregular directional case. (a) corresponds to the theoretical spectrum. (b) corresponds to the measured spectrum.

running accurate coastal applications and the correct treatment of long simulations.

Reliable wave generation and stability of the active wave absorption system have been achieved. In that vein, a new method to set the VOF in the mesh allowing fractional values has been implemented. The newly coded wave generation boundary condition includes the most widely used theories, which cover the full spectrum of water waves, and both first and second order wave generation. It also features a special condition to simulate piston-type wavemaker velocity profile, allowing direct laboratory test replication. Furthermore, as sea states are random and three dimensional, one of the advances presented is the capability of generating any frequency-direction

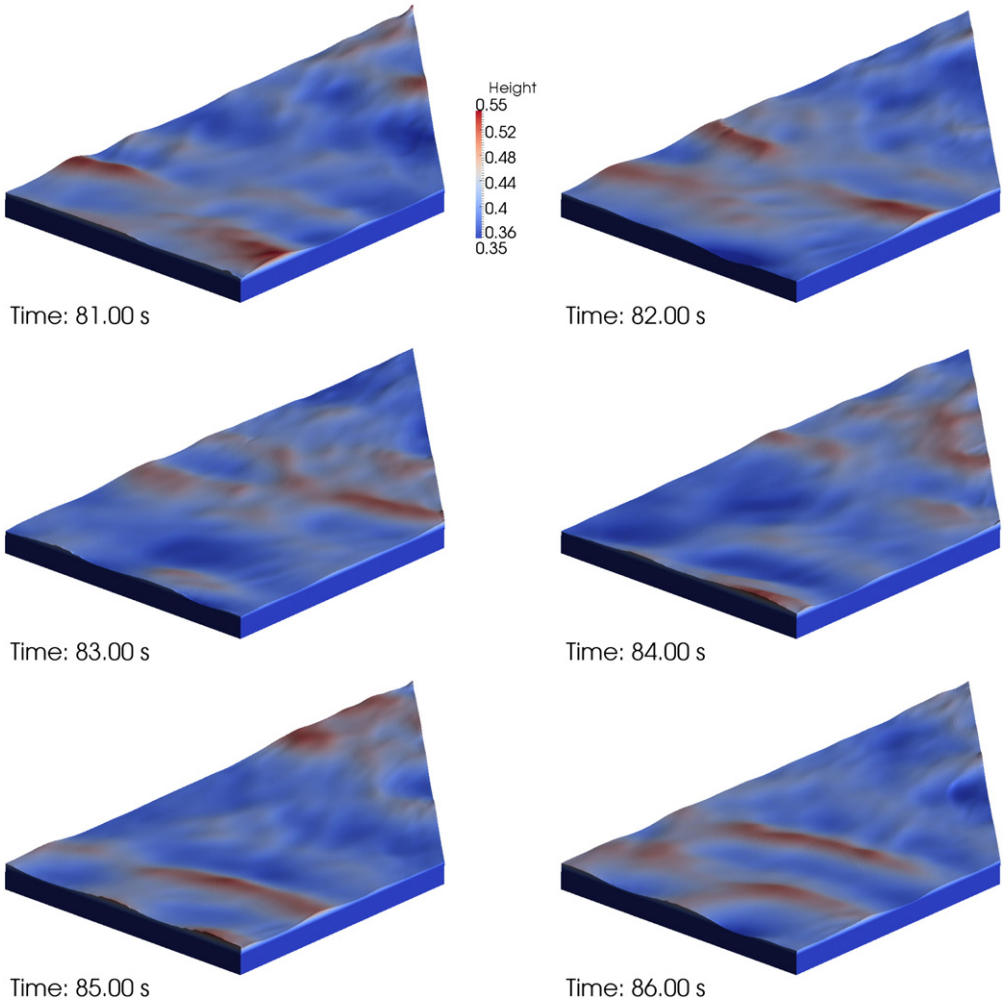

Fig. 15. Free surface for the irregular directional case. Height in m.

wave spectrum discretised in its components. Additionally, the linked active wave absorption enhances stability by decreasing the energy of the system and corrects the increasing water level of long simulations due to the excess of water in the wave crests.

The newly implemented active wave absorption has proven to be stable and to present very low reflection coefficients. Hence, it is advantageous with respect to dissipation zones such as sponge layers, as it does not increase the computational domain. Additionally, neither does increase the computational cost significantly when present. Most of the obtained reflection coefficients are well below 10%. Whenever 2D absorption theory is not applicable because it radiates waves instead of absorbing them, a new 3D theory for wave absorption has been implemented. This one shows good performance for incidence angles close to 0°or 90°, although it is moderately reflective in between. These two mentioned theories only absorb in the perpendicular direction to the boundary. Quasi-3D theory shows the clear advantage of absorbing in almost any direction. Its main drawback is that most of the times the incident wave direction cannot be anticipated or that it may vary within the same boundary.

In conclusion, OpenFOAM®, together with the newly developed boundary conditions for simultaneous wave generation and active wave absorption, constitutes an adequate choice to address coastal engineering problems. An extensive validation considering different relevant coastal engineering processes is presented in the second part of this paper (Higuera et al., in press).

Table 5
Irregular waves in a wave tank: spectra comparison. SDF stands for spectral density function.

	Sea		Swell	
	Theoretical	Measured	Theoretical	Measured
f (Hz)	0.6758	0.5950	0.1960	0.2257
θ (°)	31.17	31	27.15	19
SDF (m^2 s)	0.001538	0.001967	0.005540	0.006256

Acknowledgements

Pablo Higuera is indebted to the University of Cantabria for the funding provided in the Predoctoral Fellowships Programme.

J. L. Lara is indebted to the M.E.C. for the funding provided in the "Ramón y Cajal" Programme (RYC-2007-00690). The work is funded by projects BIA2008-05462, BIA2008-06044 and BIA2011-26076 of the "Ministerio de Ciencia e Innovación" (Spain).

References

Baldock, T.E., Swan, C., Taylor, P.H., 1996. A laboratory study of non-linear surface waves on water. Philosophical Transactions of the Royal Society A 354, 649–676.
Barthel, V., Mansard, E.P.D., Sand, S.E., Vis, F.C., 1983. Group bounded long waves in physical models. Ocean Engineering 10 (4), 261–294.
Berberovic, E., van Hinsberg, N.P., Jakirlic, S., Roisman, I.V., Tropea, C., 2009. Drop impact onto a liquid layer of finite thickness: dynamics of the cavity evolution. Physical Review E 79.
Christensen, E.D., 2006. Large eddy simulation of spilling and plunging breakers. Coastal Engineering 53 (5–6), 463–485.

Christensen, M., Frigaard, P., 1994. Design of absorbing wave-maker based on digital filters. Proceeding of Waves — Physical and Numerical Modelling, Vancouver.
Dean, R.G., Dalrymple, R.A., 1991. Water wave mechanics for engineers and scientists. Advanced Series on Ocean Engineering. World Scientific, Singapore.
del Jesus, M., Lara, J.L., Losada, I.J., 2012. Three-dimensional interaction of waves and porous coastal structures. Part I: Numerical model formulation. Coastal Engineering 64, pp. 57–72.
Fenton, J.D., 1988. The numerical solution of steady water wave problems. Computers & Geosciences 14 (3), 357–368.
Higuera, P., Lara, J.L. & Losada, I.J., in press. Simulating coastal engineering processes with OpenFOAM®. Coastal Engineering, ELSEVIER. http://dx.doi.org/10.1016/j.coastaleng.2012.06.002.
Hur, D.-S., Lee, K., Yeom, G., 2008. The phase difference effects on 3-D structure of wave pressure acting on a composite breakwater. Ocean Engineering 35 (17–18), 1826–1841.
Jacobsen, N.G., Fuhrman, D.R., Fredsøe, J., in press. A wave generation toolbox for the open-source CFD library: OpenFoam®. International Journal for Numerical Methods in Fluids. http://dx.doi.org/10.1002/fld.2726.
Jasak, H., 1996. Error analysis and estimation for the finite volume method with applications to fluid flows. Ph.D. thesis, Imperial College of Science, Technology and Medicine.
Kissling, K., Springer, J., Jasak, H., Schütz, S., Urban, K., Piesche, M., 2010. A coupled pressure based solution algorithm based on the volume-of-fluid approach for two or more immiscible fluids. V European Conference on Computational Fluid Dynamics, ECCOMAS CFD.
Lara, J.L., Garcia, N., Losada, I.J., 2006. RANS modelling applied to random wave interaction with submerged permeable structures. Coastal Engineering 53, 395–417.
Lara, J.L., Ruju, A., Losada, I.J., 2011. Reynolds Averaged Navier–Stokes modelling of long waves induced by a transient wave group on a beach. Proceedings of the Royal Society A 467, 1215–1242.
Lara, J.L., del Jesus, M., Losada, I.J., 2012. Three-dimensional interaction of waves and porous coastal structures. Part II: Experimental validation. Coastal Engineering 64, pp. 26–46.
Le Méhauté, B., 1976. Introduction to Hydrodynamics and Water Waves. Springer-Verlag, New York.
Lee, J.J., Skjelbreia, E., Raichlen, F., 1982. Measurement of velocities in solitary waves. Journal of Waterway, Port, Coastal, and Ocean Engineering 108, 200–218.
Li, T., Troch, P., De Rouck, J., 2004. Wave overtopping over a sea dike. Journal of Computational Physics 198 (2), 686–726.
Longuet-Higgins, M.S., Stewart, R., 1960. Change in the form of short gravity waves on long waves and tidal currents. Journal of Fluid Mechanics 8, 565–583.
Losada, I.J., Gonzalez-Ondina, J.M., Diaz, G., Gonzalez, E.M., 2008. Numerical simulation of transient nonlinear response of semi-enclosed water bodies: model description and experimental validation. Coastal Engineering 55 (1), 21–34.
Lubin, P., Vincent, S., Caltagirone, J.-P., Abadie, S., 2003. Fully three-dimensional direct numerical simulations of a plunging breaker. Comptes Rendus Mecanique 331 (7), 495–501.
Luppes, R., Veldman, A.E.P., Wellens, P.R., 2010. Absorbing boundary conditions for wave simulations around offshore structures. Proceedings ECCOMAS CFD 2010. Paper 1200.
Mansard, E.P.D., Funke, E.R., 1980. The measurement of incident and reflected spectra using a least squares method. Coastal Engineering 154–172.
Mendez, F.J., Losada, I.J., Losada, M.A., 2001. Wave-induced mean magnitudes in permeable submerged breakwaters. Journal of Waterway, Port, Coastal, and Ocean Engineering 127, 7–15.
Newman, J.N., 2010. Analysis of wave generators and absorbers in basins. Applied Ocean Research 32 (1), 71–82.
Pengzhi, L., Liu, P.L.-F., 1999. Internal wave-maker for Navier–Stokes equations models. Journal of Waterway, Port, Coastal, and Ocean Engineering 125, 207–215.
Rusche, H., 2002. Computational fluid dynamics of dispersed two-phase flows at high phase fractions. Ph.D. thesis, Department of Mechanical Engineering, Imperial College of Science, Technology & Medicine, London.
Sand, S.E., 1982. Long waves in directional seas. Coastal Engineering 6, 195–208.
Schäffer, H.A., Klopman, G., 2000. Review of multidirectional active wave absorption methods. Journal of Waterway, Port, Coastal, and Ocean Engineering 88–97 (March/April).
Skjelbreia, L., Hendrickson, J.A., 1960. Fifth order gravity wave theory. Proceedings 7th Coastal Engineering Conference, pp. 184–196.
Svendsen, I.A., 2006. Introduction to nearshore hydrodynamics. Advanced Series on Ocean Engineering. World Scientific, Singapore.
Torres-Freyermuth, A., Lara, J.L., Losada, I.J., 2010. Numerical modelling of short- and long-wave transformation on a barred beach. Coastal Engineering 57, 317–330.
Troch, P., De Rouck, J., 1999. An active wave generating-absorbing boundary condition for VOF type numerical model. Coastal Engineering 38 (4), 223–247.
Wang, Z., Zou, Q., Reeve, D., 2009. Simulation of spilling breaking waves using a two phase flow CFD model. Computers & Fluids 38 (10).
Wei, G., Kirby, J.T., 1995. Time-dependent numerical code for extended Boussinesq equations. Journal of Waterway, Port, Coastal and Ocean Engineering 121 (5), 251–261.
Wellens, P., 2012. Wave simulation in truncated domains for offshore applications. Ph.D. thesis, Delft University of Technology.
Wellens, P., Luppes, R., Veldman, A.E.P., Borsboom, M.J.A., 2009. CFD simulations of a semi-submersible with absorbing boundary conditions. Proceedings of the International Conference on Offshore Mechanics and Arctic Engineering, 5, pp. 385–394.
Weller, H.G., 2002. Derivation, modelling and solution of the conditionally averaged two-phase flow equations. Technical Report TR/HGW/02. Nabla Ltd.
Young, I.R., 1994. On the measurement of directional wave spectra. Applied Ocean Research 16, 283–294.